

Study on the Ultimate Bearing Capacity of Riveted Nodes of Holding Pole

Yongjun Xia^{1, a}, Lijiang Sun^{1, b}, Fanhao Meng^{1, c}, Jie Pan^{1, d}

China Electric Power Research Institute, Beijing 100055, China

^axiayj@epri.sgcc.com.cn, ^bsljiang1990@163.com, ^cmeng87123@126.com, ^dgoingjie@163.com

Abstract. The ultimate load carrying capacity of the holding pole nodes is one of the decisive factors to measure the load carrying performance of the holding pole. In order to study the ultimate load carrying capacity of riveted connection nodes of holding pole, we calculated and analysed the overall force of holding pole under different working conditions based on the finite element method, so that we extracted the real force information of the nodes, and investigated the force forms and regulations of the nodes. Based on this, the simulation of the node force characteristics was carried out, and the node ultimate load capacity test was carried out using a five-axis linkage hydraulic loading device, and the reliability of the numerical model was verified through the comparative analysis of the test and simulation results. By adjusting the riveting layout, the design of riveted joint nodes was optimised, the ultimate load capacity of the riveted nodes of the holding pole was increased up to 10.9%.

Keywords: Holding pole; riveted node; bearing capacity; simulation; optimization.

1. Introduction

Power transmission tower is an important part of the transmission line, it is usually used various types of holding poles to complete the tower set up lifting [1, 2]. Holding pole is a kind of lightweight lifting equipment, its bearing structure is assembled by multiple sections of truss-type standard section through riveted connection, which has the advantages of light weight, easy to install and dismantle, simple operation and high lifting efficiency. The riveted connection node between the standard sections of the holding rod plays the role of connecting the converging rods and transferring the load, thus its safety is very important [3]. Once the connection node fails, the connected rods will lose part or all of the bearing capacity, which may cause the change of force transmission path, local damage to the structural system, and even trigger the destruction of the continuity of the whole system [4, 5]. At present, the permissible stress method is generally used in the design of connecting nodes of holding poles [6, 7]. The permissible stress method takes the maximum load that the structure may withstand as the design load, and takes a single safety factor as the design criterion, which is difficult to deal with the safety and uncertainty under the complex coupling conditions such as different loads and different operating characteristics, resulting in high margin and large weight in the design of the holding pole node [8, 9]. Therefore, it is necessary to research on the ultimate load carrying capacity of holding pole riveted connection nodes [10].

In this paper, it was taken a certain type of double rocker landing pole as the object of study, firstly, the whole finite element model of the pole was established, and the whole force of the pole was calculated and analysed under all kinds of working conditions. Subsequently, the real force information of the riveted connection nodes between the standard sections of the holding pole was extracted, and the force forms and regulations of the nodes were studied and determined. Then the local finite element model of the node was established, and the ultimate load bearing performance of the node was analysed according to the force characteristics of the node; Based on the simulation study, the five-axis linkage hydraulic loading device was used to carry out the ultimate load bearing capacity test of the riveted connection node of the holding pole. Finally, by optimising the local layout of the riveted connection, the ultimate load carrying capacity of the riveted connection node of the holding pole is improved.

2. Simulation Analysis of Holding Pole Node Force Characteristics

Taking the 44m all-steel internal floating holding pole (ZB-D-38/800/60) as the research object, the whole structure of the holding pole was analysed by numerical simulation. According to the design parameters of aluminium alloy holding pole (listed in Table 1) to establish the holding pole finite element model, as shown in Figure 1.

Since the standard section of ZB-D-38/800/60 aluminium alloy holding pole is connected by riveting between the sections, as shown in Figure. 1, so the paper mainly studies the riveted nodes for aluminium alloy holding pole.

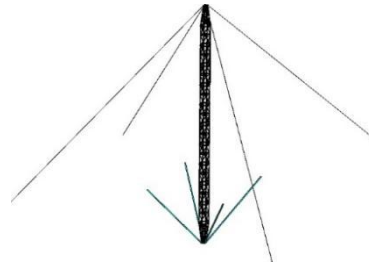


Fig. 1 Nodal model of riveted aluminium alloy holding pole
Table 1. The main parameters of aluminium alloy holding pole

Items	Parameters
Separate height	44m
Rated lifting torque	48t·m
Maximum unbalance torque	16t·m (33.3% of rated lifting moment)
Maximum lifting weight	4t (working range of 1.5~12m)
Working range	Minimum range of 1.5m (angle of 87°), maximum range of 12m (angle of 3°)
Cross-section of standard section for holding pole	650mm×650mm
Main chord	∟ 100×8
Straight web bar	∟ 56×5
Diagonal web rod	∟ 50×4
Straight web bar at the end of the standard section	∟ 70×5
Aluminium alloy material	2A12, Elastic modulus of 207GPa, Poisson's ratio of 0.3
Material of steel wire rope	Elastic modulus of 120GPa, Poisson's ratio of 0.3

The main chord, straight web and diagonal web of the holding bar are modelled by the BEAM188 units (3D linear finite strain beams), and the connection between the bars was rigid. The luffing ropes were simulated with LINK180 cells (3D tension-only or compression-only rods), and the connection with the main body of the holding pole was hinged.

Three typical working conditions (as shown in Table 2) were selected to analyse the force law of the rod nodes in the holding pole.

Table 2. Typical load conditions for a double rocker arm holding pole

Working condition	Tilt angle of the right boom (°)	Load on the right (t)	Tilt angle of the left boom (°)	Load on the left side (t)	Wind load (N)
1	10	8	10	8	3690
2	5	8	5	8	3690
3	5	4	5	4	3690

Take working condition 1 as an example to analyse the force process of the whole structure of the holding pole. From the axial force graph in Figure 2, it can be seen that the tension and pressure of the main chord near the riveted connection node between the standard sections of the holding

pole body was the largest, with the maximum pressure of 56kN and the maximum tensile force of 25 N. Since the main chord at the riveted node only suffered from pressure, the riveted connection node at the maximum pressure was the most unfavourable node on the main chord of the holding pole body.

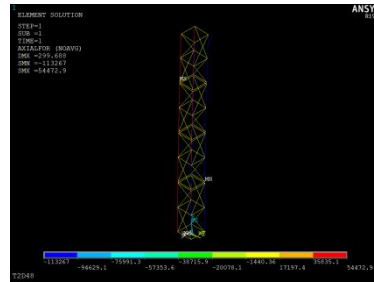


Fig. 2 Axial force diagram of the body of a double-rocking arm drop holding pole (unit: N)

The main chord bar of the riveted connection node was subjected to pressure action only. Therefore, the axial force, maximum shear force, axial stress and maximum bending stress of the riveted connection rods on the main chord bar of the hugger near the maximum and minimum axial pressures were extracted from the finite element analysis results, and the results were shown in Table 3 and Table 4, and the riveted connection node rods were numbered, as shown in Figure 3.

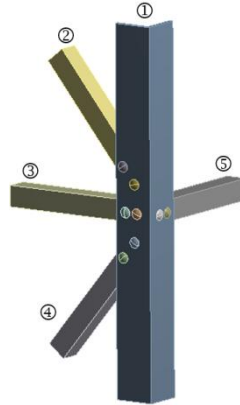


Fig. 3 Rod numbering of the riveted node model for the holding pole

Table 3. Force analysis of the bar at the riveted node at the maximum pressure on main chord bar in working condition 1 (load is 6t, inclination angle is 10°)

Numbering of bars	Axial force (kN)	Shear force (kN)	Axial stress (MPa)	Bending stress (MPa)
①	-56.95	-0.625	-37	3.6
②	-1.085	-0.01	-2	-1.2
③	0.941	-0.008	2.5	-1.4
④	-2.13	0.018	-4.1	-0.47
⑤	1.25	-0.021	3.3	-2.1

Table 4 Force analysis of bar at riveted node at minimum pressure of main chord bar in working condition 1 (load is 6t, inclination angle is 10°)

Numbering of bars	Axial force (kN)	Shear force (kN)	Axial stress (MPa)	Bending stress (MPa)
①	-25.03	-0.36	-16	-3.5
②	-0.75	-0.013	-1.4	-0.7
③	1.03	-0.012	2.6	-1.2
④	-1.98	0.022	-3.8	-0.7
⑤	0.72	-0.011	2	-0.3

The holding pole of the other two working conditions in Table 2 was analysed by force analysis respectively, and the force information of each pole was extracted as shown in Table 5 and Table 6.

Table 5. Force analysis of the bar at the riveted node at the maximum pressure on main chord bar in working condition 2 (load is 6t, inclination angle is 5°)

Numbering of bars	Axial force (kN)	Shear force (kN)	Axial stress (MPa)	Bending stress (MPa)
①	-43.2	-0.5	-28	3.6
②	-1.1	-0.014	-2.1	-1.2
③	0.95	-0.01	2.5	-1.6
④	-1.86	0.018	-3.5	-0.2
⑤	1.01	-0.016	2.6	-1.9

Table 6. Force analysis of the bar at the riveted node at the maximum pressure on main chord bar in working condition 3 (load is 4t, inclination angle is 5°)

Numbering of bars	Axial force (kN)	Shear force (kN)	Axial stress (MPa)	Bending stress (MPa)
①	-32.78	-0.36	-21	-5.3
②	-0.57	-0.005	-1.1	-0.6
③	0.53	0.003	1.4	-0.8
④	-1.23	0.01	-2.4	-0.2
⑤	0.62	-0.049	1.6	-1.2

It can be concluded from Table 3 to Table 6 that the node was subjected to axial force, shear force and bending moment at the same time, in which the axial force of the bar was much larger than the shear force applied to the bar, and the axial stress of the bar was larger than the maximum bending stress of the bar. Therefore, it is enough to consider only the axial loading force in the finite element simulation and test of the load carrying capacity of the riveted connection node of the holding pole.

In addition, under different working conditions, the holding pole riveted nodes in the maximum axial pressure position of the rod force form was consistent, the distribution of the axial force value of the rod was with regularity, σ , $\&$, \bullet , \circ and \blacksquare axial force ratio of -50:-1:1:-1:-2:1. Therefore, in the following finite element simulation of the ultimate load bearing capacity of the holding pole node and test, the rod loading mode were used in the above form of force and the value of the force ratio.

3. Study on the Strength Failure and Whole Body Instability Problem

In order to accurately determine the ultimate load bearing capacity of the node, the reason for the failure of the riveted node under pressure conditions should be correctly analysed, whether it was strength failure or member instability.

According to the stability calculation formula for axial compression members in GB50429:

$$\frac{N}{\bar{\varphi} \times A} \leq f \quad (1)$$

Where N is the design value of axial pressure; A is the gross cross-sectional area; $\bar{\varphi}$ is the stability coefficient of axial compression members, f is the design value of the yield strength of the aluminium alloy material, for the non-welded uniaxial symmetric cross-section exists the following equation:

$$\bar{\varphi} = \eta_e \times \eta_{as} \times \varphi \quad (2)$$

φ is the aluminium alloy axial compression member stability coefficient, and its expression is shown in Equation 3.

$$\varphi = \frac{1 + \eta + \bar{\lambda}^2}{2\bar{\lambda}^2} - \sqrt{\left(\frac{1 + \eta + \bar{\lambda}^2}{2\bar{\lambda}^2}\right)^2 - \frac{1}{\bar{\lambda}^2}} \quad (3)$$

The $\bar{\lambda}$ is the relative length to slenderness ratio of the member.

$$\bar{\lambda} = \frac{\lambda \sqrt{f_{0.2} / E}}{\pi} \quad (4)$$

According to the calculation based on the riveted node, the critical force for whole instability is shown in Equation 7:

$$N = f \times \bar{\varphi} \times A = 99.26 \text{ kN} \quad (5)$$

4. Finite Element Analysis of Ultimate Bearing Capacity of Holding Pole Nodes

From the above analysis, it can be seen that the riveted connection nodes of the holding pole were only subjected to pressure, and the pole body was subjected to the greatest pressure at the riveted connection nodes, so the results of the main parameters of the riveted connection nodes of the extracted aluminium alloy holding pole (ZB-D-38/800/60) which was shown in Table 7.

Table 7. Parameters of rivet connection nodes for holding pole

Diameter of rivet hole d_0	Number of shear surface m	Thickness of riveted part δ	Strength of 2A01 rivet		Strength of riveted part 2A12	
			Design strength f_m^b	shearing strength f_m^c	Design strength δ_{mp}	compressive strength δ_{mc}
8.2mm	1	4mm	110MPa	190MPa	213MPa	390MPa

According to DL/T 319-2018 “General Technology of Holding Pole for Overhead Transmission Line Construction”, the material of ZB-DL-25/650/30 aluminium alloy holding pole was Q355, and the standard section of the holding pole was riveted connection between the sections, and the riveting specification was M22, and the other parameters were shown in Table 7.

Holding pole standard section rod force transmission path was mainly axial force transmission, according to the riveted connection node configuration, the ultimate load bearing condition was mainly axial pressure on the main chord rod. The aluminium alloy holding pole riveted node ultimate load bearing condition according to the pole ①, pole ②, pole ③, pole ④ and pole ⑤ axial force ratio of -50:-1:1:-1:-2:1 for multi-axial loading. The multi-axial forces were loaded to the force values in Table 8, and the axial limit loading values were shown in Table 8 when buckling occurred at the flange of the main chord bar near the diagonal web bars 3 and 4. The first order buckling load factor was 1.155, and since the applied load to the main bar was 100 kN, it was known that the buckling critical force of the main bar was $100 \times 1.155 = 115.5$ kN, and its deformation diagram was shown in Figure 4. In order to simplify the calculation, the mesh size was 3mm, so the buckling critical force calculated by finite element was in error with the theoretical calculation. In this case, the maximum stress of the bar in the static analysis of finite element was 285 MPa, which did not reach the yield limit stress of 2A12 material 300 MPa, as shown in Figure 5. The maximum shear stress of the rivet was 28.9 MPa, which did not reach the shear strength of 190 MPa of 2A01 type rivet, as shown in Figure 6. It is indicated that the reason for the failure of node 2 was the whole instability of the main rod according to the results of finite element calculation.

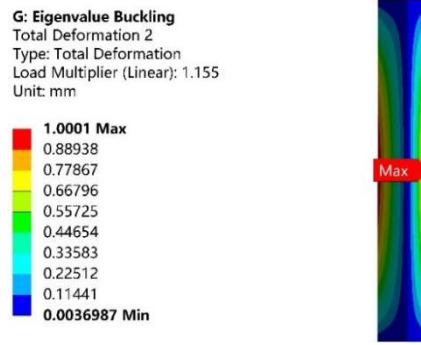


Fig. 4 First order flexural modal deformation of the riveted node bar

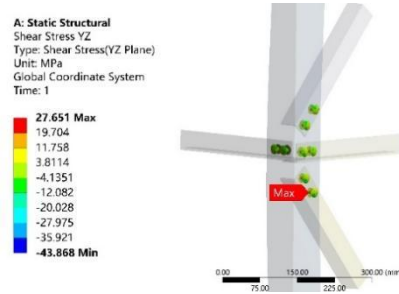
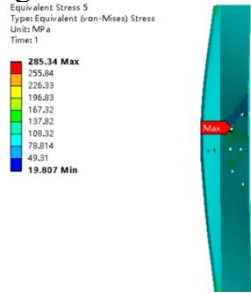


Fig. 5 Stress diagram of riveted node bar Fig. 6 Stress diagram of riveted node bar rivet
Table 8. The critical force values for riveted nodes of aluminium alloy holding pole in buckling (node 2)

Numbering of bars	①	①	②	③	④	⑤
Ultimate carrying capacity (kN)	End fixed	-100	-2	2	-4	2

5. Ultimate Load Capacity Test of Riveted Joint Node of Holding Pole

5.1 Test Platform

Experimental research is the earliest and most adopted research method in the study of structural nodes. By using the test method to study the elastic stress distribution, ultimate strength and deformation of nodes under static loading, it can not only collect more reliable node bearing information, but also adjust the theoretical analysis model according to the test results and measure the quality of the analysis method.

In order to accurately test the regularity of strain development on the nodes, the strain gauges were arranged on the unfavourable parts of the test specimen nodes according to the results of finite element simulation analysis. The strains of all parts were collected by TS8132 dynamic strain gauges, and 20mm range LVDT displacement gauges were arranged in the node area of the test specimen for determining the elongation of the node ends of the rods along the direction of the force, and for monitoring the displacements of the nodes in the thin parts of the nodes. The axial ultimate bearing capacity of the nodes was collected and recorded by the force transducers embedded in the test loading equipment.

In order to make the forces on the nodes effective, a five-axis linkage hydraulic loading device was used for the test, as shown in Figure 7. The main chord of the loading device was fixed at one end, and the rest of the rod ends were connected to the loader, and the centre of the rod cross-section was opposite to the axis of the loader, so as to keep the axis of the rod under force. A bidirectional hydraulic cylinder was used in the loader to achieve movement in both directions of stretching and pressing. As shown in Figure 8, when the multiaxial force was loaded until the rod deformed significantly, the loading was stopped and the data of the whole loading process was recorded.

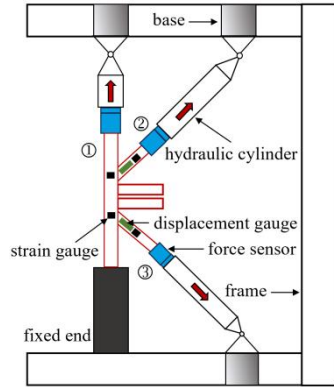


Figure 7. Sketch of the loading test setup

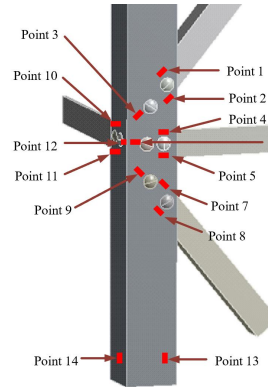


Figure 8. Location of stress points

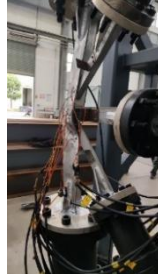
5.2 Result Analysis

After the end of the force application test, the buckling of the main chord in the riveted connection area of transverse web 3 and diagonal web 4, and in the riveted connection area of transverse web 5 appeared firstly, as shown in Figure 9 (a) ~ (c), which were typical of the overall instability situation, and the location of the nodes where the buckling occurred was almost the same as that in the finite element simulation results.

The stress change of riveted joint nodes during loading was shown in Figure 10 (a) ~ (d) was the change curve of applied axial force during loading. In the test data, the stress curves of measurement points 4~6 and 7~9 were the first to change at 560s, and the results are shown in Figure 10 (a) ~ (b). As shown in Figure 10 (c), the stress at measurement points 13 and 14 were 300MPa at 1000s, which reached the material yield limit of 2A12 aluminium alloy rod, and the axial loading force was 202.5kN at 1000s. From this, it can be concluded that the buckling of main chord bar occurred before yielding, and the ultimate load capacity of riveted joint node obtained from the test was 107.5kN.



(a) The whole structure damage state

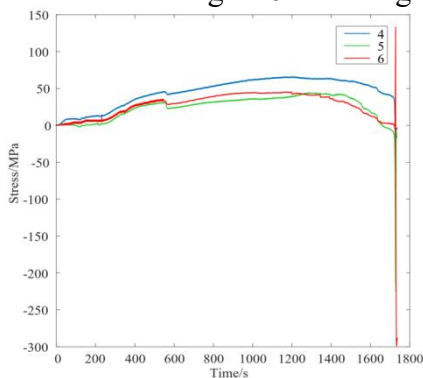


(b) Local damage state 1

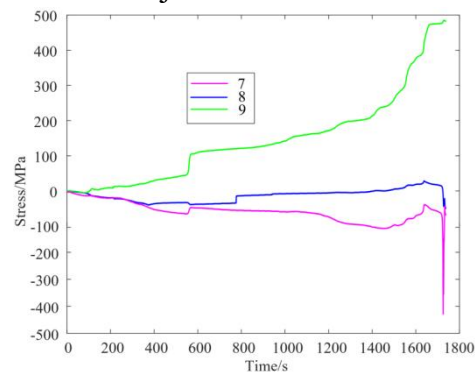


(c) Local damage state 2

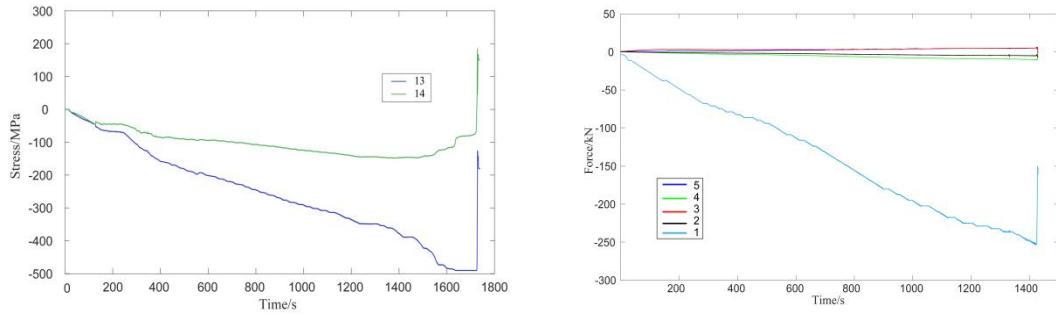
Figure 9. Loading test results of riveted joint nodes



(a) Stresses at nodes 4~6



(b) Stresses at nodes 7~9



(c) Stresses at nodes 13~14 (d) Loading axial force based on hydraulic cylinders

Figure 10. Test data of riveted joint nodes

By comparing the simulated and experimental values of the ultimate bearing capacity of riveted joint nodes, the following conclusions can be obtained:

(1) As shown in Figure 10 (a), the overall instability started to happen when the axial force at measurement points 4~6 and 7~9 was loaded to 107.5kN at 560s, and then reached the yield limit when the axial force was loaded to 202.5kN at 1000s. The loading force value of the diagonal web bar 4 was greater than that of the diagonal web bar 2, and thus the deformation position of node 2 was on the side close to the diagonal web bar 4 rather than on the side close to the diagonal web bar 2.

(2) As shown in Figure 10 (b) ~ (c), there was a buckling deformation of the main chord located in the area of the rivet connection between rod 3 and rod 4, and the same was true for the main chord located in the area of the rivet connection of rod 5, so that the rivets at the deformed position were subjected to bending moments after the rods were buckled, and the rivets here were subjected to shear and tensile forces at the same time, which led to fracture.

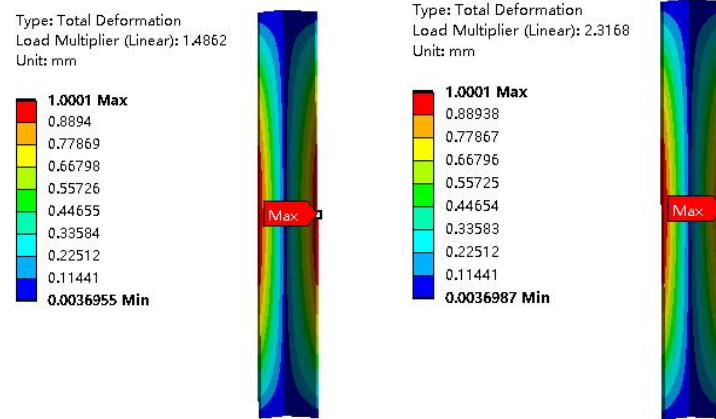
(3) The buckling critical force in the test data was 107.5kN, which was a certain error from the theoretical calculation and finite element analysis results. The reason for the error is that in the theoretical calculation and finite element analysis, the force on the main chord bar was much larger than that on the other web bars, so the buckling critical force of the main chord bar was calculated separately in the model and the other web bars were neglected.

6. Optimised Design of Riveted Connection Nodes for Holding Pole

For the instability problem of aluminium alloy structure, the main influencing factors included the length to thickness ratio of the member, the width to thickness ratio of the plate, the cross-section configuration, the material properties, the geometric initial defects, etc. In this paper, the main chord bar wall was thickened to adjust the length to thickness ratio of the member, and the rivet number was adjusted by the design method to enhance the local stability of the node.

Figures 11 (a) and (b) respectively showed the deformation of the riveted node main chord bar wall thickness of 7mm and 8mm nodes when they reached the ultimate load carrying state. The first-order buckling load factors were 1.486 and 2.317, and the buckling critical forces of the corresponding rods were 148kN and 232kN, which respectively increased the ultimate load carrying capacity by 48% and 132%. It can be seen that the ultimate load carrying capacity of the node can be significantly improved by increasing the wall thickness of the main chord bar. The ultimate load carrying capacity of each bar when node 2 reached the ultimate working condition was listed in Table 9.

Increasing the number of rivets in the node 2 at the connection between the main bar and the web bar to 3 or 4 can improve the stress distribution and avoid stress concentration. The Table 10 showed the ultimate bearing capacity of each bar when the riveted nodes reached the ultimate working condition.



(a) Thickness of 7 mm (b) Thickness of 8 mm

Fig 11. First order flexural modal deformation of the bar after reinforcement at node 2

Table 9. Ultimate load capacity of Node 2 bars after increasing the wall thicknesses

Thickness of wall	Numbering of bars	①	②	③	④	⑤
7mm	Ultimate carrying capacity (kN)	-148	-2.96	2.96	-5.92	2.96
8mm	Ultimate carrying capacity (kN)	-232	-4.64	4.64	-9.28	-4.64

Table 10. Ultimate load capacity of Node 2 bars after increasing the number of rivets

Number of rivets	Numbering of bars	①	②	③	④	⑤
3	Ultimate carrying capacity (kN)	-72.5	-1.575	1.575	-3.15	1.575
4	Ultimate carrying capacity (kN)	-78.8	-1.65	1.65	-3.3	-1.65

7. Summary

In this paper, the force form of nodes in the whole holding rod was obtained by analysing the force characteristics of nodes, and the ultimate load bearing condition of nodes was simulated by adopting the method of multi-axial equiproportional step-by-step loading until node destruction. Through the finite element analysis, the ultimate bearing capacity of each node was obtained, and the ultimate bearing performance of the nodes of the holding rod was tested based on the finite element simulation, then the following conclusions can be obtained:

- (1) The failure damage of riveted nodes was overall instability problem rather than strength problem;
- (2) The damage location of the riveted node under compression was located on the main chord in the area of the riveted connection of rods 3 and 4, and also on the main chord in the area of the riveted connection of rod 5;
- (3) The main reason for the failure of rivets at the riveted nodes was due to the combined action of the bending moment and shear force on the rivets after the overall instability and buckling of the main chord;
- (4) According to the finite element analysis results, the ultimate bearing capacity of the member can be improved by adjusting the wall thickness. Since the stress region was mainly concentrated on the main chord, the number of rivets was adjusted to improve the stress distribution to avoid stress concentration.

References

- [1] Zhi-Jun Y, Gang Z, Jin W. Pole and Tower Planning for Three Gorges-Shanghai ± 500 kV DC Transmission Line[J]. Electric Power Construction, 2008.

- [2] Shu Q, Yuan G, Huang Z, et al. The behaviour of the power transmission tower subjected to horizontal support's movements[J]. *Engineering Structures*, 2016, 123.
- [3] Porcaro R, Langseth M, Hanssen G, et al. Crashworthiness of self-piercing riveted connections[J]. *International Journal of Impact Engineering*, 2008, 35(11): 1251-1266.
- [4] Wenxuan P. Determination of Limit Bearing Capacity of Soil Anchor Rods by Method of Limit Analysis[J]. *Geotechnical Investigation & Surveying*, 2004.
- [5] Heinemeyer C, Feldmann M. The influence of rivet corrosion on the durability of riveted connections[J]. *Steel Construction*, 2011, 4(3): 188-192.
- [6] Bennett R M. Allowable Stress Design Method for Flexural Reinforcement in Shear Walls[J]. *The Masonry Society journal*, 2017, 35(1): 47-47.
- [7] Li D, Han L, Shergold M, et al. Influence of Rivet Tip Geometry on the Joint Quality and Mechanical Strengths of Self-Piercing Riveted Aluminium Joints[J]. *Materials Science Forum*, 2013, 765: 746-750.
- [8] Kluger K, Lagoda T. Fatigue life of metallic material estimated according to selected models and load conditions[J]. *Journal of Theoretical & Applied Mechanics*, 2013, 51(3): 581-592.
- [9] Imam B, Righiniotis T, Chryssanthopoulos M. Connection fixity effects on stress histories in riveted rail bridges[J]. 2011.
- [10] Zhi-Gang M A. Ultimate Load-carrying Capacity Study of Three Steel Pipe Latticed Column[J]. *Construction & Design for Project*, 2005.